PHYSICAL REVIEW E VOLUME 49, NUMBER 2 FEBRUARY 1994

Optical determination of the saddle-splay elastic constant K_{24} in nematic liquid crystals

R. D. Polak, G. P. Crawford, B. C. Kostival, J. W. Doane, and S. Žumer*
Liquid Crystal Institute, Kent State University, Kent, Ohio 44242-0001
(Received 13 October 1993)

Nematic liquid crystals confined to supramicrometer capillary tubes with homeotropic anchoring conditions are studied using optical polarizing microscopy. The resulting microscopy textures are sensitive to the molecular anchoring strength W_θ and the saddle-splay surface elastic constant K_{24}. These two quantities are determined by comparing the observed textures of the escaped-radial nematic director field to simulated textures predicted from Frank elastic theory and considering the stability ranges of other possible structures.

PACS number(s): 61.30.−v, 62.20.Dc, 07.60.Pb, 64.70.Md

Elastic continuum theory, proposed by Oseen and Zocher [1] and Frank [2], successfully describes bulk elastic distortions in nematic liquid crystals when surface or field constraints are imposed. Specific constants, K_{11}, K_{22}, and K_{33}, describe the three basic distortion modes: splay, twist, and bend, and many experiments have been devised to measure them [3]. Ericksen [4] first treated theoretically the effect of the saddle-splay surface elastic constant K_{24} on the stability of the nematic director field, deriving inequalities of K_{24} with respect to K_{11}, K_{22}, and K_{33}; however, the saddle-splay elastic constant K_{24} eluded measurement. The inherent difficulties in measuring K_{24} arise from the simultaneous presence of bulk distortions and the effects of surface anchoring. The value of K_{24} was recently measured in submicrometer cylindrical cavities filled with nematic liquid crystal using deuterium nuclear magnetic resonance [5] and in periodic structures observed with optical polarizing microscopy in hybrid aligned nematic layers [6]. The constant K_{24} compared in magnitude to the splay, twist, and bend elastic constants. The importance of the mixed-splay-bend surface elastic contribution (K_{13}) is attracting a great deal of theoretical interest [7–14] and remains a topic of intense controversy.

We present an optical method to measure K_{24} and the polar molecular anchoring strength W_θ. It is based on the sensitivity of the escaped-radial director field, stable in capillary tubes with homeotropic anchoring conditions, to the dimensionless surface parameter σ defined by [15]

$$\sigma=\frac{RW_\theta}{K_{11}}+\frac{K_{24}}{K_{11}}-1\ , \tag{1}$$

where R is the radius of the capillary tube. An optical polarizing microscope is used to study the details of the escaped-radial director field for various radii. The observed optical birefringence textures are directly compared to theoretical patterns which simulate the interference of ordinary and extraordinary light after phase shifts occurring while passing through structures predicted from elastic theory [16]. *A priori* knowledge of the ordinary n_o and extraordinary n_e indices of refraction for the liquid crystal, as well as the elastic constant ratio K_{33}/K_{11}, allows for the simultaneous determination of W_θ/K_{11} and K_{24}/K_{11}.

The director field of nematic liquid crystals constrained to a small cavity in zero field depends on the interplay between molecular surface anchoring and elastic energies. As our discussion is limited to supramicrometer size capillary tubes, the approximation of a constant order parameter S throughout the volume of the capillary is justified. The free energy of a confined liquid crystal is then given by [17]

$$F_e=\tfrac{1}{2}\int_{\text{vol}}\{K_{11}(\nabla\cdot\mathbf{n})^2+K_{22}(\mathbf{n}\cdot\nabla\cdot\mathbf{n})^2+K_{33}(\mathbf{n}\times\nabla\times\mathbf{n})^2 -K_{24}\nabla\cdot(\mathbf{n}\times\nabla\times\mathbf{n}+\mathbf{n}\nabla\cdot\mathbf{n})\}d +\tfrac{1}{2}W_\theta\int_{\text{surf}}\sin^2\phi\,dA\ , \tag{2}$$

where K_{11}, K_{22}, K_{33}, and K_{24} are the Frank elastic constants and $\mathbf{n}$ represents the local direction of the optic axis of the uniaxial nematic liquid crystal. The constant W_θ denotes the molecular surface anchoring strength, while ϕ is the angle between the actual nematic director $\mathbf{n}$ and the preferred molecular orientation at the surface. The K_{24} contribution of the free energy can be reduced to a surface integral by Gauss's theorem. We totally ignore the mixed-splay-bend term in Eq. (2) associated with the K_{13} coefficient based on consistently keeping terms of first derivatives of $\mathbf{n}$ and the presence of weak deformations of the director field [7,8]. Incorporating K_{13} into Eq. (2) would require a more complex treatment of the Frank free energy which involves the higher-order derivatives of the director field [14] or performance of an infinite sum of higher-order terms as recently reported [12].

For cylindrical cavities, several stable nematic director-field configurations depend on anchoring conditions. Here we study nontwisted structures with homeotropic anchoring, such as escaped-radial configurations, whose nematic director can be completely specified by $\mathbf{n}=\sin\Omega(r)\mathbf{e}_r+\cos\Omega(r)\mathbf{e}_z$ where Ω is the angle between $\mathbf{n}$ and the cylindrical axis (see Fig. 1). Given $k=K_{33}/K_{11}$ and σ (K_{22} is not required since there is no twist deformation), the escaped-radial director field can be predicted by minimizing the free energy. The molecular anchoring angle at the cavity wall of a cylindrical tube of radius R is determined to be [15]

*Permament address: Department of Physics, University of Ljubljana, Jadranska, 19, 61000, Ljubljana, Slovenia.

$$\Omega(r=R)=\cos^{-1}\left[\frac{k^{1/2}}{(\sigma^2+k-1)^{1/2}}\right] \tag{3}$$

and the explicit relation for $\Omega(r)$ is [15]

$$\frac{r}{R}=\left[\frac{\sigma+1}{\sigma-1}\right]^{1/2}\left[\frac{\Delta-\beta'\cos\Omega(r)}{\Delta+\beta'\cos\Omega(r)}\right]^{1/2} \times\exp\left[\frac{\beta}{\beta'}U[k,\Omega(r)]\right]\exp\left[-\frac{\beta}{\beta'}U[k,\Omega(r)]\right] \tag{4}$$

with

$$U[k,\Omega(r)]=\begin{cases}\sin^{-1}[\beta\cos\Omega(r)], & k>1\\ -\sinh^{-1}[\beta\cos\Omega(r)], & k<1\end{cases} \tag{5}$$

where $\Delta=[1-\beta^2\cos^2\Omega(r)]^{1/2}$, $\beta^2=|k-1|/k$, and $\beta'^2=1/k$. In a particular case ($K_{11}=K_{22}=K_{33}=K$), the free energy per unit length of the escaped-radial configuration is [4,15]

$$F_{ER}=\pi K\left[3-\frac{K_{24}}{K}-\frac{1}{\sigma}\right]. \tag{6}$$

Another stable nematic director-field configuration for homeotropic boundary conditions is the planar-polar configuration [4,15] which occurs for small values of RW_θ/K_{11}. Our experiments were performed in large enough cavities so that we did not encounter this configuration. Not observing the planar-polar structure, however, provides a means to determine the lower bound on K_{24}/K_{11} as will be discussed later. The free energy per unit length of this configuration in the one-constant approximation is [4,15]

$$F_{PP}=\pi K[-\ln(2\xi\gamma)+(1-\gamma)/\xi], \tag{7}$$

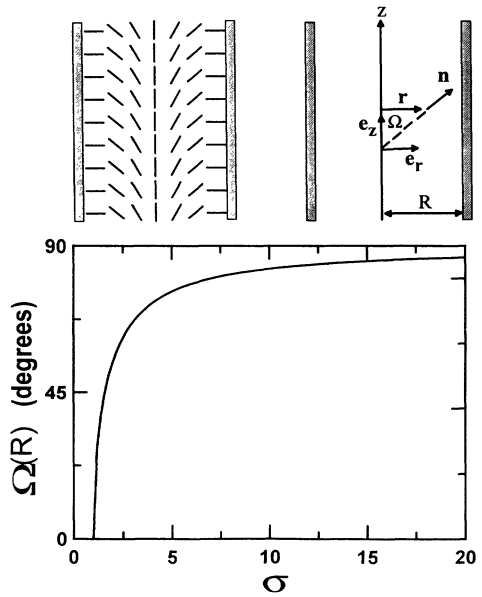

FIG. 1. Nematic director-field pattern for the escaped-radial configuration next to the coordinate system used to describe the configuration (above). The graph below shows the surface anchoring angle at the capillary wall for the escaped-radial director field as a function of σ using $K_{33}/K_{11}=1.5$. As σ approaches infinity, the surface anchoring angle asymptotically approaches 90° (i.e., strong anchoring).

where $\xi=2K/RW_\theta$ and $\gamma=(\xi^2+1)^{1/2}-\xi$.

Capillary tubes of radii ranging from 5 to 25 μm were filled with nematic-liquid-crystal mixture E7 and 5CB (4′-pentyl-4-cyanobiphenyl), both available from EM Chemicals. The capillary tubes were pretreated with lecithin (Sigma Chemical Co.) to promote homeotropic surface anchoring. The filled tubes were surrounded by a glycerin matrix with index of refraction n_m equal to the glass of the capillary tubes [16]. The samples were placed between the crossed polarizers of an optical microscope. Mercury and sodium monochromatic light sources, $\lambda_0=435$ and 589 nm, respectively, were used to extract details about the nematic director fields.

The observed microscope textures occur after the interference of ordinary and extraordinary components of light phase shift as they pass through the polarizer, capillary tube and liquid crystal, and the analyzer. A transformation matrix $\mathbf{P}(r)$, described in our previous paper [16], is used to express the resulting intensity of transmitted light by

$$I(\mathbf{r})=\|\mathbf{e}_A P(\mathbf{r})\mathbf{e}_P\|^2, \tag{8}$$

where $\mathbf{e}_A$ is the orientation of the analyzer, $\mathbf{e}_P$ is the orientation of the polarizer, and r is the distance from the center of the cylinder. We ignore deviations of light rays resulting from reflection from cavity walls and refraction through the liquid crystal since n_e-n_o, $n_e-n_m \ll n_m$. For details on this methodology, see Ondris-Crawford *et al.* [18], Scharkowski *et al.* [19], and Xu, Kitzerow, and Crooker [20], who calculated droplet textures in a similar way.

The optical microscope textures are calculated for the incident light wave vector $\mathbf{k}_0$, being perpendicular to the

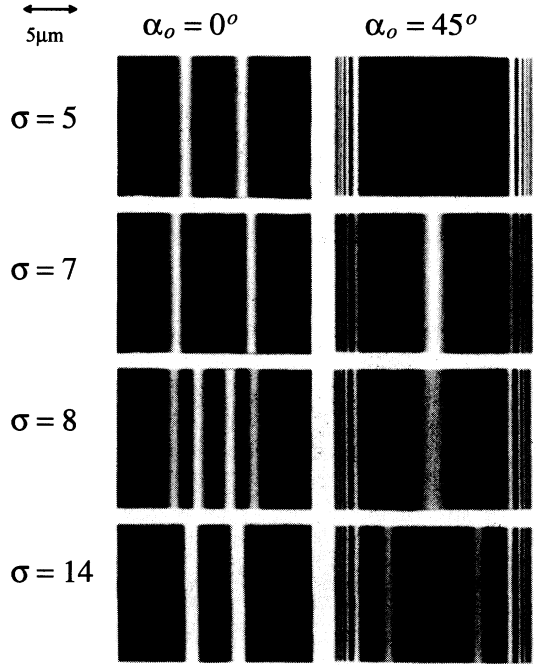

FIG. 2. Simulated textures of a nematic liquid crystal confined to a cylindrical tube of radius 10 μm with $\lambda_0=435$ nm; the material parameters are particular to E7. The value of σ is varied, while all of the other variables in the simulation are held fixed.

symmetry of axis of the sample. The computer-simulated texture is calculated according to Eqs. (4), (5), and (8); the input parameters are $n_e, n_o, \lambda_0, R, \alpha_0$ (the orientation of the initial polarization vector), K_{33}/K_{11}, and σ. Figure 2 gives an example of the effects of σ, while keeping the other variables constant. Note that while large changes in σ yield very different textures, small changes have only minor influence.

The nematic mixture E7 has the following material parameters: $K_{33}/K_{11}=1.54$, $K_{22}/K_{11}=0.93$; for $\lambda_0=435$ nm, $n_e=1.8208$ and $n_o=1.544$; and for $\lambda_0=589$ nm, $n_e=1.5239$ and $n_o=1.7424$. 5CB has the following material parameters: $K_{33}/K_{11}=1.4$, $K_{22}/K_{11}=0.66$, $n_e=1.7947$, and $n_o=1.556$ and for $\lambda_o=589$ nm, $n_e=1.5308$ and $n_o=1.7230$ [21]. The optical birefringence textures were compared to the computer simulations for each radius and two different light sources. The best fit for σ was made by analyzing four different textures (two with $\lambda_0=435$ nm at $\alpha_0=0°$ and 45° and two with $\lambda_0=589$ nm at $\alpha_0=0°$ and 45°) at each radius by matching the number of fringes and fringe position, and relative intensity of the fringes. Figures 3 and 4 show the optical microscope textures for two different radii against the computer simulations at the determined best fit for σ. The manufacturer's specification on capillary tube radius, ± 1 μm, was unacceptable for the delicacy of our experiment; therefore scanning electron microscope measurements were made to confirm the radius for each tube.

Figure 5 gives the values of σ vs the capillary tube radii for E7 and 5CB. Since σ is a linear function of the capillary radius R, we use linear regression to determine W_θ/K_{11}, while the ordinate axis intercept will yield K_{24}/K_{11}. For E7, W_θ/K_{11} lies between 0.37 μm^{-1} and 0.69 μm^{-1}, with a best fit of 0.56 μm^{-1}, and the K_{24}/K_{11} ratio for E7 falls between 1.3 and 5.2 with a best-fit value of 2.6. For 5CB, we found W_θ/K_{11} to fall between 0.74 μm^{-1} and 1.6 μm^{-1} with a best fit of 1.1 μm^{-1} and K_{24}/K_{11} to lie between -2.1 and 7.5 with a best fit of 3.1. We expected the 5CB data to have larger errors than E7 since W_θ/K_{11} is stronger as reflected in the steeper slope in Fig. 5.

Taking into account stability considerations one can limit the possible K_{24} values to a much narrower interval. In the first step, the Ericksen inequality $0<K_{24}<2K_{11}$ or $2K_{22}$ (whichever is smaller), valid for nematic phases where no spontaneous ordering occurs, is used. In the second step we take into account that the planar-polar configuration was not observed and estimate a lower bound of K_{24} by comparing the free energy of planar and escaped structure. To use the planar-polar configuration described by Eq. (7), we approximate $K\sim(K_{11}+K_{33})/2$. From our experiment when $R=5$ μm we found W_θ/K to lie between 0.37 μm^{-1} and 0.69 μm^{-1} as determined (see Fig. 5). We estimate the lower bound on K_{24}/K for E7 to be 1.6 and the upper to be 1.9. Applying this same logic to 5CB, we found the lower bound on K_{24}/K to be 1.2

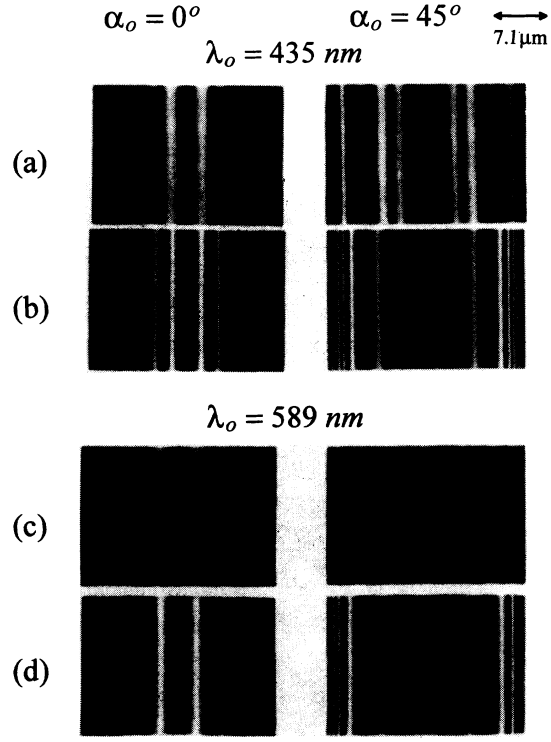

FIG. 3. Polarizing microscopy photographs (black and white) (a) and (c) compared with computer simulated textures (b) and (d) for a $R=14.25$ μm capillary tube filled with the nematic liquid crystal E7 viewed between crossed polarizers using a monochromatic mercury light source (a) and (b) and sodium light source (c) and (d). The simulations correspond to $\sigma=11$.

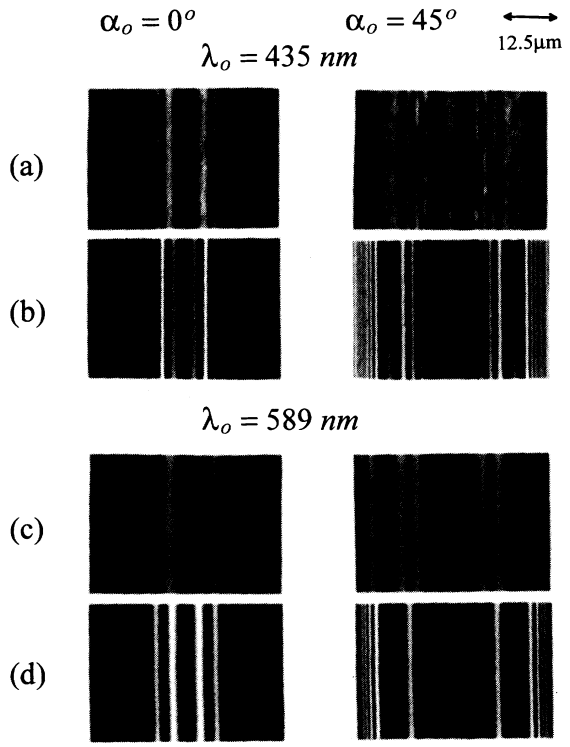

FIG. 4. Polarizing microscopy photographs (black and white) (a) and (c) compared with computer simulated textures (b) and (d) for a $R=25$ μm capillary tube filled with the nematic liquid crystal E7 viewed between crossed polarizers using a monochromatic mercury light source (a) and (b) and sodium light source (c) and (d). The simulations correspond to $\sigma=15$.

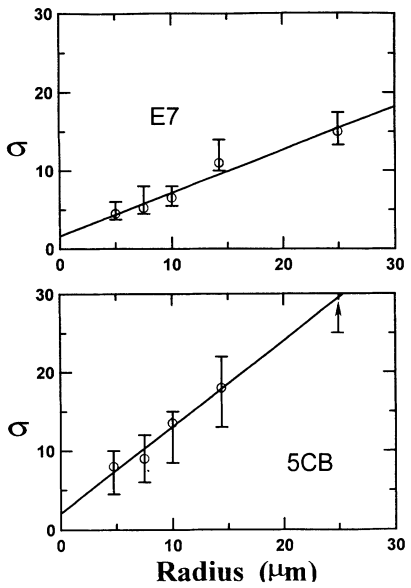

FIG. 5. This graph shows σ as a function of capillary tube radius for E7 (top) and 5CB (bottom). The circles correspond to the best possible fit for each data point, and the error bars represent acceptable values of σ for each radius. The lines represent a linear regression through the data points giving values of W_θ/K_{11} (slope) and K_{24}/K_{11} (ordinate axis intercept plus 1). The 5CB data point for $R=25$ μm represents a lower bound for possible values of σ. No best-fit data point could be obtained since the simulated texture becomes much less sensitive when $\sigma > 25$.

and 1.6, respectively. (See Table I.)

Combining stability and structural considerations we conclude that in both cases $K_{24} \sim 2K_{22}$. Results within the experimental error compare favorably with our previous work [4,5,15], and a recent study by Sparavigna, Lavrentovich, and Strigazzi [6] on 5CB gives K_{24} to be similar to the bulk elastic constants. The value of the anchoring strength for 5CB confined in lecithin-treated Nuclepore membranes [4,15] was determined to be $W_\theta/K=6\pm1$, approximately 5 times larger than our $W_\theta/K=1.1\pm0.5$ for 5CB confined to lecithin-treated glass capillaries. The discrepancy can be attributed to the one-constant approximation employed in analyzing the Nuclepore-5CP data, different surface treatment procedures, or different underlying substrates.

TABLE I. Summary of surface anchoring and surface elastic parameters.

Liquid crystal	W_θ/K_{11} $(\mu m)^{-1}$	W_θ[a] (J/m^2)	K_{24}/K_{11}	$K_{24}/K >$[b]	$K_{24}/K <$[c]
E7	0.56	6.1×10^{-6}	2.6	1.6	1.9
5CB	1.1	6.6×10^{-6}	3.1	1.2	1.6

[a]Using $K_{11}=1.1\times10^{-11}$ J/m for E7 and $K_{11}=6.0\times10^{-12}$ J/m for 5CB.
[b]Lower bound calculation based on a stability consideration in the one-constant approximation.
[c]Upper bound calculated from Ericksen inequality with $K=(K_{22}+K_{11})/2$.

Our optical technique does not require sophisticated instrumentation to measure the molecular anchoring strength W_θ and the saddle-splay surface elastic constant K_{24}. In this optical determination of K_{24}, direct observation of the nematic director fields and stability arguments are combined. The K_{24} constant is important in nematic director-field configurations in spherical droplets and cylindrical capillaries [4,5,15,17,20], stripe configurations [22], and hybrid aligned nematic cells [6,23]. Our method can be further improved by substituting the comparison of the simulated textures and photographic pictures with a comparison between measured and calculated intensities of the transmitted light [19].

This research was supported by the National Science Foundation (NSF) under Solid State Chemistry Grant No. DMR91-20130 and NSF Science and Technology Center ALCOM DMR89-20147.

[1] C. W. Oseen, Trans. Faraday Soc. **29**, 883 (1933); H. Zocher, Trans. Faraday Soc. **29**, 945 (1933).
[2] F. C. Frank, Discuss. Faraday Soc. **25**, 19 (1958).
[3] P. R. Gerber and M. Schadt, Z. Naturforsch. **35a**, 1036 (1980).
[4] J. L. Ericksen, Phys. Fluids **9**, 1205 (1966).
[5] R. Ondris-Crawford, G. P. Crawford, S. Žumer, and J. W. Doane, Phys. Rev. Lett. **70**, 194 (1993); D. W. Allender, G. P. Crawford, and J. W. Doane, *ibid.* **67**, 1442 (1991).
[6] O. D. Lavrentovich, Phys. Scr. **T39**, 394 (1991), A. Sparavigna, O. D. Lavrentovich, and A. Strigazzi, Phys. Rev. E **49**, 1344 (1994).
[7] J. Nehring and A. Saupe, J. Chem. Phys. **54**, 337 (1971); **56**, 5527 (1972).
[8] C. Oldano and G. Barbero, Phys. Lett. **110A**, 213 (1985); Mol. Cryst. Liq. Cryst. **168**, 1 (1989); **170**, 99 (1989); G. Barbero, *ibid.* **195**, 199 (1991).
[9] H. P. Hinov, Mol. Cryst. Liq. Cryst. **148**, 197 (1987); **178**, 53 (1990).
[10] V. H. Schmidt, Phys. Rev. Lett. **64**, 535 (1990).
[11] N. V. Madhasudana and R. Pratibha, Mol. Cryst. Liq. Cryst. **179**, 207 (1990).
[12] V. M. Pergamenshchik, Phys. Rev. E **47**, 1881 (1993); **48**, 1254 (1993); V. M. Pergamenshchik, P. I. C. Teixeira, and T. J. Sluckin, *ibid.* **48**, 1265 (1993).
[13] G. Barbero and G. Durand, Phys. Rev. E **48**, 1942 (1993).
[14] D. W. Allender (unpublished).
[15] G. P. Crawford, D. W. Allender, and J. W. Doane, Phys. Rev. A **45**, 8693 (1992).
[16] G. P. Crawford, J. A. Mitcheltree, E. P. Boyko, W. Fritz, S. Žumer, and J. W. Doane, Appl. Phys. Lett. **60**, 3226 (1992).
[17] S. Žumer and S. Kralj, Liq. Cryst. **12**, 613 (1992).
[18] R. Ondris-Crawford, E. P. Boyko, B. G. Wagner, J. H. Erdmann, S. Žumer, and J. W. Doane, J. Appl. Phys. **69**, 6380 (1991).
[19] A. Scharkowski, G. P. Crawford, S. Žumer, and J. W. Doane, J. Appl. Phys. **73**, 7280 (1993).
[20] F. Xu, H. S. Kitzerow, and P. P. Crooker, Phys. Rev. A **46**, 6535 (1992).
[21] BDH Chemicals Ltd., Poole, Dorset, England BH12 4NN.
[22] G. Srajer, F. Lonberg, and R. B. Meyer, Phys. Rev. Lett. **67**, 1102 (1991).
[23] A. Sparavigna, L. Komitov, O. D. Lavrentovich, and A. Strigazzi, J. Phys. II (France) **2**, 1881 (1992).

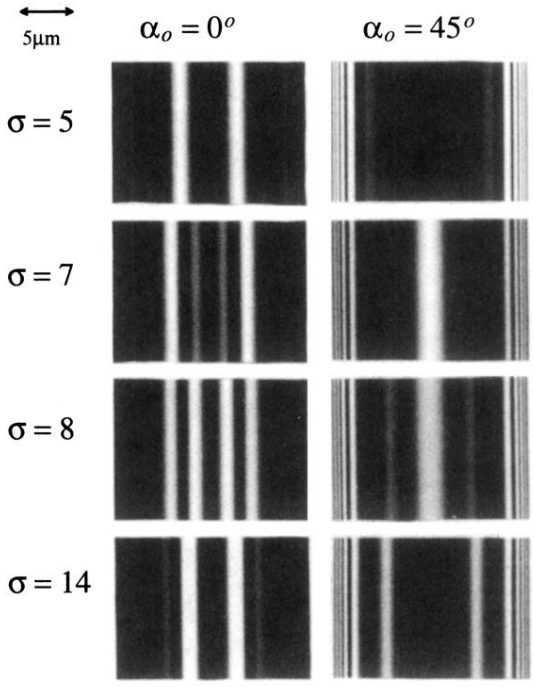

FIG. 2. Simulated textures of a nematic liquid crystal confined to a cylindrical tube of radius 10 μm with λ_0=435 nm; the material parameters are particular to E7. The value of σ is varied, while all of the other variables in the simulation are held fixed.

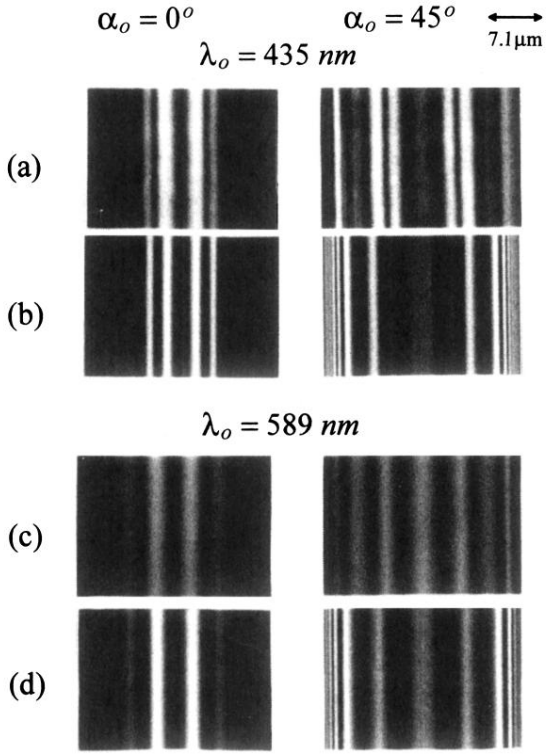

FIG. 3. Polarizing microscopy photographs (black and white) (a) and (c) compared with computer simulated textures (b) and (d) for a $R = 14.25\ \mu$m capillary tube filled with the nematic liquid crystal E7 viewed between crossed polarizers using a monochromatic mercury light source (a) and (b) and sodium light source (c) and (d). The simulations correspond to $\sigma = 11$.

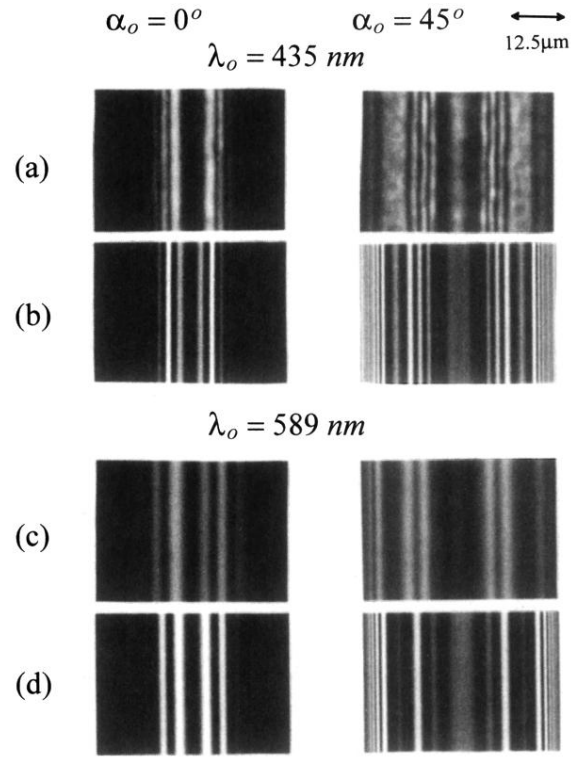

FIG. 4. Polarizing microscopy photographs (black and white) (a) and (c) compared with computer simulated textures (b) and (d) for a $R = 25\ \mu$m capillary tube filled with the nematic liquid crystal E7 viewed between crossed polarizers using a monochromatic mercury light source (a) and (b) and sodium light source (c) and (d). The simulations correspond to $\sigma = 15$.